Journal of Applied Electrochemistry **32**: 951–960, 2002.

Electrocatalytic removal of dissolved oxygen from seawater in a packed-bed electrode

P. KINZEL[1], H-G. LINTZ[1], P. GAUDEBERT[2], G. BOUSQUET[2], F. LAPICQUE[1] and G. VALENTIN[1,*]
[1]*Laboratoire des Sciences du Génie Chimique, CNRS-ENSIC, F-54001 Nancy, France*
[2]*Total Fina–Elf, F-69120 Solaize, France*
*(*author for correspondence, e-mail: Gerard.Valentin@ensic.inpl-nancy.fr)*

Received 21 January 2002; accepted in revised form 29 May 2002

Key words: carbon materials, electrocatalytic reactors, oxygen reduction, packed-bed electrode

Abstract

Oxygen dissolved in seawater is the source of severe corrosion issues in off-shore platforms for oil exploitation. The electrocatalytic reduction of dissolved oxygen from seawater was investigated at laboratory scale as an alternative to the current processes for the removal of oxygen. Due to the low concentration of dissolved oxygen and the very high conversion required before use of seawater in off-shore platforms, the reduction has been carried out in a packed–bed electrode consisting of carbon-based particles of various nature. The reduction involves the intermediate formation of peroxide species whose further reduction into hydroxyl ion is a slow process on Pt-free surfaces. A continuous laboratory packed-bed electrode was designed and tested in long-term operations for the assessment of the production and the reaction selectivity. The removal of oxygen from seawater can be inhibited by the formation of a solid $CaCO_3$–$Mg(OH)_2$ film at the carbon particles, which favours the accumulation of peroxide species. However, this electrode deactivation can be avoided at sufficient polarisation.

1. Introduction

Oil recovery from oilfields can be enhanced by the injection of steam or water in the liquid layers and this technique is widely used, in particular for off-shore exploitations. Injection of seawater from off-shore platforms is the source of severe corrosion issues in the injection pipes, because of the presence of dissolved oxygen. In addition, the hydrated oxides of metals formed by corrosion can lead to the clogging of the oilfield pipes. Seawater is therefore treated prior to its injection into the oilfields, and the process used for this purpose has to allow the oxygen concentration to be reduced from about 9 to 10 ppb. The flow rate of seawater to be treated is about 5000 $m^3\ h^{-1}$ per exploitation well.

Stripping at reduced pressures or by gas injection is now the leading technique [1, 2]; however all gases cannot be used for this purpose, and for instance, the use of carbon dioxide results in significant decrease of the water pH. The outlet concentration of oxygen in the liquid is in the range 20–40 ppb and a secondary reduction by sulfite is required. In addition the liquid is stripped in 20 m high towers. Even if further developments [3] seem to avoid the additional treatment by chemical reaction and to reduce considerably the height of installation, alternative processes are under study. The catalytic reduction by hydrogen is one of these alternative techniques, but its application is hindered by the large volume of the catalytic reactor (around 40 m^3), the cost of the noble metals acting as catalysts, and the upstream electrolyser required for hydrogen production [4]. Electrocatalytic reactors allow the electrochemical reduction step to be combined with the catalytic reduction of oxygen: the catalytic material acts as a cathode for this purpose, and a significant reduction in the volume of the treatment unit may be expected.

The present paper reports the investigation of the electrocatalytic removal of oxygen from seawater in a laboratory scale cell. The electrochemical reaction was carried out at the surface of carbon-based catalysts because of the moderate costs of these materials. Three-dimensional electrodes appear to be the most suitable devices because of the low concentration of dissolved oxygen in water, the moderate current density to be applied, and the high conversion to be attained in large-scale processes for the treatment of seawater.

2. Physicochemical data of the systems used

2.1. *Main features of seawater*

The composition of seawater depends to some extent on its origin, and the present investigation was focused on seawater drawn from Byfjord in Norway at 40 to 80 m deep, which is representative of the conditions of the

off-shore oilfields in the North Sea. Selected physico-chemical data of the seawater used are reported in Table 1 [5]. The average temperature of seawater at 80 m is around 10 °C, within a few degrees, depending on the period of the year. In most cases, the oxygen concentration at 80 m varies from 65 to 85% of the saturation concentration. For the present investigation, the saturation concentration of oxygen will be considered at 9.0 ppm [5].

Seawater is an aqueous solution of various salts as shown in Table 2. The main cations are sodium, magnesium, calcium, and potassium to a lower content; in addition to the chloride anion, seawater contains also sulfate, hydrogencarbonate, bromide, and fluoride ions. Transition metals (e.g., iron, copper, zinc, lead and nickel) are also present at ppm levels or below (Table 2). Preliminary experiments were carried out with synthetic solutions of analytical grade sodium chloride (Prolabo, France) at 32.1 g l^{-1}.

2.2. *Electrocatalytic materials*

The electrochemical reduction of oxygen is effective on carbon materials, transition metals and noble metals with a view to a large-scale process for oxygen reduction, carbon materials (e.g., graphite or activated carbons) were tested. Graphite (S797 grade, Carbone Lorraine, France) was in the form of irregular grains with a mean diameter near 2.5 mm. Its high density corresponds to a low BET area (Table 3). Two activated carbons (CECA, Paris, France) in the form of irregular grains (NC35) or cylindrical pellets (BGP), were also used: their main features are summarised in Table 3.

Platinum-impregnated graphite (1 wt %) was prepared in the Laboratoire de Catalyse en Chimie Organique (UMR CNRS 6503, Poitiers, France) from S797 graphite allowing the noble metal to be dispersed in nanometer-sized clusters. A second Pt-doped material was purchased from Degussa (Hanau, Germany): it consisted of cylindrical pellets of activated carbon with a BET area near 350 m^2 g^{-1}, yielding 20 nm Pt clusters dispersed on the porous structure, and with a metal content near 1%.

The electrical conductivity of the packed bed of catalyst particles was measured by impedance spectroscopy using a 20 mm × 20 mm × 20 mm cell provided with two facing platinum electrodes (20 mm × 20 mm). The cell was previously calibrated with KCl solutions in the concentration domain 0.001–1.00 M [6]. After introduction of the carbon particles into the cell, the packed-bed arrangement was improved by using an ultrasonic bath for one minute before applying a mechanical pressure of about 1 bar, i.e. at a reasonable level for the brittle particles. Spectra were recorded from 20 kHz to 1 Hz: the imaginary part of the impedance was negligible at frequencies above 1 kHz, and the real component varied within 2% only in the high frequency domain. The overall experiment was repeated several times for assessment of the accuracy of the technique. Although efficient for liquid solutions and for beds of small beads, the technique is of moderate accuracy for the largest particles as for the Pt-impregnated graphite pellets, and the data given in Table 3 have to be considered as orders of magnitude, only.

Table 1. Physico-chemical properties of seawater at 10 °C [5]

Property	Value
Salinity/g l^{-1}	33–36
pH	8–8.6
Electrical conductivity/mS cm^{-1}	38.3
Density/kg m^{-3}	1028
Viscosity/mPa s	1.45

Table 2. Typical composition of seawater [5]

Cation	Concentration /ppm	Anion	Concentration /ppm
Na^+	10 160	Cl^-	19 350
Mg^{2+}	1250	SO_4^{2-}	2710
Ca^{2+}	413	HCO_3^-	142
K^+	387	Br^-	67
Sr^+	8	F^-	1
Fe(II), Fe(III)	1–3		
Zn^{2+}	0.6		
Cu^{2+}	0.2		

2.3. *Electrochemical reactions*

Carbon materials are efficient catalysts for the reduction of oxygen into peroxide and the overall current is proportional to the oxygen concentration and to the BET area, below 100 m^2 g^{-1} [7]. The rate-determining step is the first electron transfer, namely the formation of $(O_2)^-_{ads}$ species on graphite electrodes immersed in alkaline media, or the generation of an HO_2 radical from adsorbed oxygen on other carbon materials [7, 8]. Peroxide ions are fairly stable on carbon surfaces and their further reduction into water and hydroxide ions is usually slow. Impregnation of carbon materials with metal particles or application of more cathodic polarisation allow the complete reduction into hydroxyl ions.

The presence of platinum in the form of nanoparticles or clusters on the electrode surface, allows the fast adsorption of oxygen, and the electrochemical formation of adsorbed HO_2 or OH radicals [9, 10] is rate controlling. In addition, hydrogen peroxide can be easily reduced into hydroxyl ion and the oxygen reduction is usually considered complete. However, the side-formation of hydrogen (Reaction 3) cannot be totally avoided on the catalyst surface, and the adsorbed hydrogen may contribute to the consumption of oxygen through the indirect process (Reaction 4). Finally, hydrogen peroxide can disproportionate into oxygen and hydroxyl ions (Reaction 5).

The overall reactions involved in the reduction of oxygen are listed below:

Table 3. Physicochemical properties of the materials used
Density values given refer to the particles, and not to packed-bed

Material	Particles	Density /g l^{-1}	BET /m^2 g^{-1}	κ /mS cm^{-1}
Graphite S797	Beads, dia. 2.5 mm	1700	<1	100 (50%)
Graphite S797 + Pt 1%	Beads, dia. 2.5 mm	>1700	<1	120 (50%)
AC/Pt 1% (Degussa)	Cylindrical pellets, dia. 2.5 mm, 2–7 mm long	800	350	8 (25%)
CECA BGP activated carbon	Irregular pellets, size 1.25–3.15 mm	300	750	3 (20%)
CECA NC35 activated carbon	Irregular beads dia. 1.5–2.5 mm	750	1200	10 (20%)

$$O_2 + H_2O + 2e^- \longrightarrow HO_2^- + OH^- \quad (1)$$

$$HO_2^- + H_2O + 2e^- \longrightarrow 3OH^- \quad (2)$$

$$Pt + H^+ + e^- \longrightarrow Pt\text{–}H_{ads} \quad (3)$$

$$4Pt\text{–}H + O_2 \longrightarrow 4Pt + H_2O \quad (4)$$

$$2HO_2^- \longrightarrow O_2 + 2OH^- \quad (5)$$

2.4. *Voltammetry of oxygen reduction*

The electrochemical behaviour of seawater saturated with oxygen was investigated at a Pt disc electrode in seawater. The voltammograms recorded on the motionless surface at 10 mV s^{-1}, exhibit conventional features depicted elsewhere [10, 11] (Figure 1). For potentials more cathodic than −0.4 V vs SCE, the current peaks correspond to the reversible adsorption and desorption of hydrogen on platinum and involving Pt–H species (zone I). The moderate current recorded in an intermediate region (II) is due to capacitive phenomena with little significant faradaic processes. For potentials beyond −0.1 V in the anodic scan (zone III), the adsorption of oxygen results in the formation of platinum oxide, as shown by the large peak of current; the irreversible reduction of the oxide and the subsequent oxygen desorption is expressed by the cathodic peak near 0.4 V.

The currents recorded on a S797 graphite disc were quite smaller, expressing the moderate activity of this carbon material, in spite of the broader potential range for the scans. The voltammograms could not be interpreted directly because of the nearly linear i/E variation, at both motionless or rotating disc electrodes. The i/E curves recorded at a graphite RDE at 400 rpm in seawater deaerated with N_2, exhibit a slow, regular increase of current from −0.25 V vs SCE, attributable to the reduction of organic groups on the carbon surface, and to the sluggish hydrogen adsorption (Figure 2). Addition of hydrogen peroxide to the deaerated liquid results in higher currents, with a well-defined current wave of normal slope from −0.65 V, and a sort of plateau is attained at −1.0 V vs SCE. Comparison of the two current variations with that recorded from seawater saturated with air oxygen (Figure 2), shows that the reduction of oxygen into peroxide occurs in a broad range of potentials from −0.30 V, whereas the peroxide species is mainly reduced in the domain −0.60 to −1.0 V vs SCE. This confirms the fair stability of hydrogen peroxide on carbon surfaces at moderate cathodic polarisation.

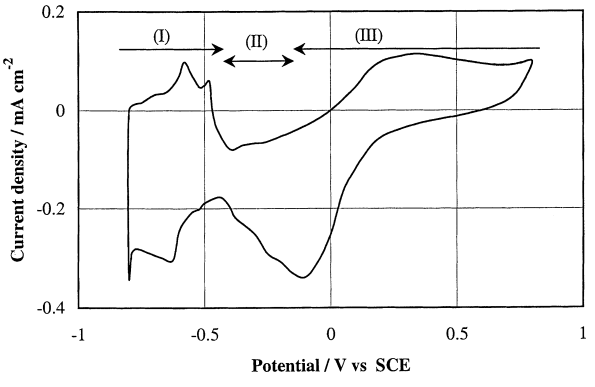

Fig. 1. Voltammetric curve on a motionless Pt disc electrode dipped in seawater saturated with air oxygen at ambient pressure and 10 °C. Scanning rate 10 mV s^{-1}.

3. Design, build-up and operation of laboratory packed-bed electrode

3.1. *Design of the packed-bed electrode*

The efficiency of the electrocatalytic route was investigated at laboratory scale using a continuously operated cell provided with a three-dimensional electrode con-

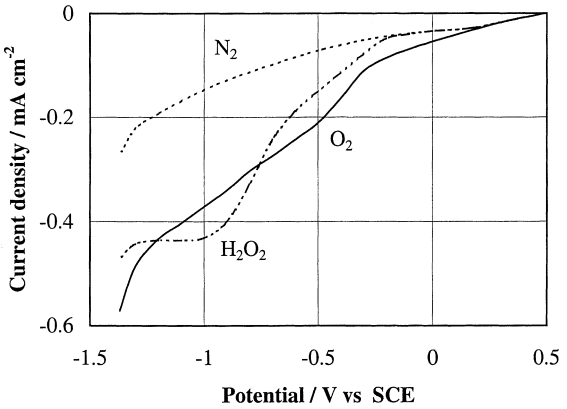

Fig. 2. Steady-state i/E curves recorded at a rotating disc electrode of graphite immersed in seawater at ambient pressure and 10 °C, depending on the nature of saturating gas (nitrogen or air oxygen), and upon addition of H_2O_2 at 110 ppm in deaerated seawater. Rotation rate 400 rpm.

sisting of a packed bed of carbon materials. The active area offered by the packed-bed electrode must be sufficient for significant abatement of dissolved oxygen from seawater. The effective oxygen reduction must also occur at appreciable rates throughout the cell, and with little hydrogen evolution. For that purpose the electrode potential may vary in a range of 500 mV as shown by voltammetric measurements. This has been confirmed by the results presented in Section 4.

The distribution of the electrode potential in a three-dimensional electrode of given dimensions was calculated following the procedure of Enriquez-Granados [12, 13], taking into account the equivalent electrical conductivity of both the solid structure, σ, and of the liquid solution, κ. The electrode potential is defined as the difference of the solid potential, Φ_S, and of that in the liquid phase, Φ_L:

$$E = \Phi_S - \Phi_L \tag{6}$$

Calculations were carried out considering the electrode arrangement shown in Figure 3, and the following assumptions were made:

(i) The oxygen reduction into hydroxyl ions is carried out under diffusion control in the entire electrode vol-ume with a 100% current yield. Therefore, the local current due to the faradaic process was written as

$$i_R = zFk_dC(y) \tag{7}$$

where $z = 4$ in the present case, k_d is the mass transfer coefficient and C denotes the local concentration of dissolved oxygen in the liquid bulk.

(ii) Plug flow conditions prevail in the packed-bed structure, with negligible dispersion in flow direction along the coordinate y. The mass balance equation in the reactor, taking into account Equation 7, leads to

$$C(y) = C_{in}\exp\left[-\frac{ak_dy}{v}\right] \tag{8}$$

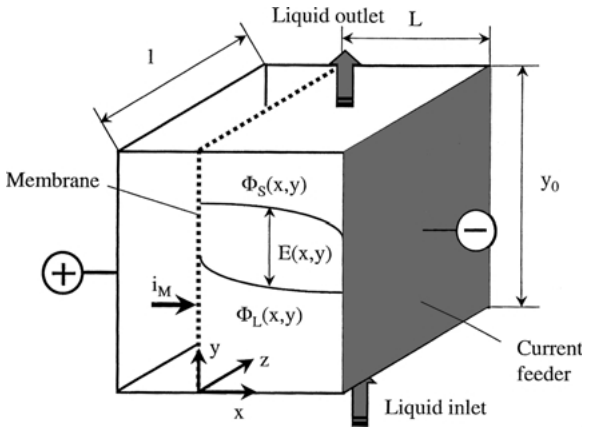

Fig. 3. Schematic view of the three-dimensional electrode for oxygen reduction.

where v is the superficial velocity of seawater in the empty channel.

(iii) the packing has uniform values for the porosity, ε, and the interfacial area, a. For spherical particles of diameter d_p, a is simply expressed by

$$a = \frac{6(1-\varepsilon)}{d_p} \tag{9}$$

The current density at the membrane, i_M, was defined as the ratio of the current through the membrane over its area; i_M is the sum of the components passing through the solid and the liquid phases:

$$i_M = i_S + i_L \tag{10}$$

The spatial variation between the electrodes of these two densities is due to the local consumption of dissolved oxygen at the carbon particles:

$$\frac{\partial i_L}{\partial x} = -\frac{\partial i_S}{\partial x} = ai_R \tag{11}$$

The distributions of potentials Φ_L and Φ_S were obtained from the charge balances written in the two phases, regardless of the transverse coordinate z (two-dimensional problem):

$$\frac{\partial^2\Phi_L}{\partial x^2} + \frac{\partial^2\Phi_L}{\partial y^2} = \frac{1}{\kappa}\frac{\partial i_L}{\partial x} \tag{12a}$$

$$\frac{\partial^2\Phi_S}{\partial x^2} + \frac{\partial^2\Phi_S}{\partial y^2} = \frac{1}{\sigma}\frac{\partial i_S}{\partial x} \tag{12b}$$

The conductivity of the solid structure was determined as explained in Section 2.2. The equivalent conductivity of the liquid in the porous medium, κ, was deduced from that of seawater, κ_0, using Bruggeman's relation.

Integration of Equation 12, taking into account Relations 7–11 and subject to the suitable boundary conditions, yielded the expressions of the potential differences $(E(x,y) - E(0,0))$ [13]. Application of the obtained formula was carried out using Dwidedi's relation [14] for mass transfer rate at the carbon particles:

$$k_d = 1.1\frac{v}{\varepsilon}\frac{Re_p^{-0.72}}{Sc^{2/3}} \quad \text{for } Re_p < 10 \tag{13a}$$

$$k_d = 0.45\frac{v}{\varepsilon}\frac{Re_p^{-0.41}}{Sc^{2/3}} \quad \text{for } Re_p > 10 \tag{13b}$$

where Re_p is the particle Reynolds number. The diffusion coefficient of dissolved oxygen was deduced from polarization curves of oxygen reduction at a Pt rotating disc immersed in seawater at 10 °C. The obtained value of 1.50×10^{-9} m^2 s^{-1} agrees well with previously published data at 1.65×10^{-9} m^2 s^{-1} at 25 °C

in a 1 M solution of NaOH [11] or KOH [15], taking into account the change in temperature and viscosity by use of the Nernst–Einstein relation. The model parameters selected for the preliminary design are $d_p = 2.5$ mm, $v = 1$ cm s^{-1}, $\varepsilon = 0.42$, $D = 1.50 \times 10^{-9}$ m^2 s^{-1} leading to $k_d = 3.41 \times 10^{-5}$ m s^{-1}, $\kappa_0 = \sigma = 38$ mS cm^{-1}, $y_0 = 35$ mm, $L = 15$ mm and $l = 30$ mm, corresponding to an expected conversion of oxygen around 15% by application of Relation 7.

The profiles of the potential differences obtained exhibit a well-pronounced symmetry over the depth of the cathode compartment (Figure 4), and the values vary from 400 to 850 mV. These profiles result from the individual potential differences in the liquid and in the solid, respectively exhibiting their maximums close to the current feeder (i.e., at $x = L$), and at the membrane surface ($x = 0$) (data not shown). As expected, the maximum differences in potential E are observed at the inlet of the cell (i.e., for the highest concentrations of the reactant) and for $x = L/2$. Although significant, the calculated differences of potential vary in a domain suitable for the efficient, selective reduction of dissolved oxygen, as discussed in Section 4.

Further calculations with other values for the particle size and the liquid velocity in the range 0.5–2 cm s^{-1}, led to comparable distributions of the electrode potential in the bed.

3.2. *Experimental set-up*

The electrochemical cell was constructed from of Perspex. The cathode consisted of the packed-bed electrode investigated above, and a Pt-coated titanium plate acting as the current feeder. An upward flow of the solution saturated with oxygen at 10 °C was passed through the packed-bed; the superficial velocity v was varied from 0.6 to 2.8 cm s^{-1}. The cathode potential was measured with respect to a reference electrode (SCE) with a thin sintered glass extension inserted in the packed-bed. The anode was a 35 mm × 30 mm titanium plate coated with ruthenium oxide at 25 g m^{-2}; this material was selected because of its high ability for oxygen evolution from acidic media. Various dilute acids were tested, and the lowest overvoltages at given current density were obtained with 1.0 M sulfuric media. The anode compartment, being 5 mm deep, was separated from the cathode packed-bed with a Nafion® 450 membrane. A stack of polymeric grids was inserted in the anode chamber to allow mechanical support to the membrane from the ambient pressure in the bed. The flow rate of sulphuric solution was fixed at 0.5 cm^3 s^{-1}.

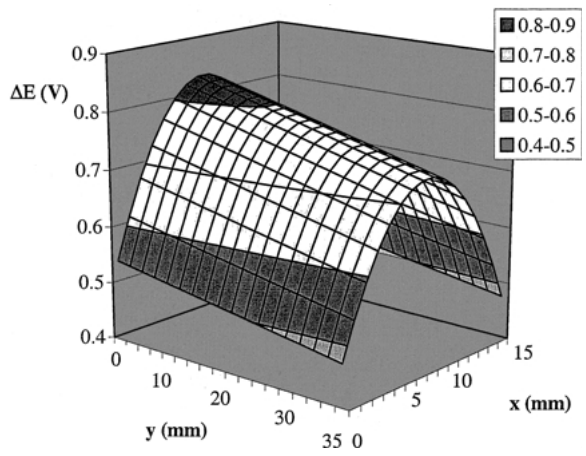

Fig. 4. Potential profile in the three-dimensional electrode, obtained by superposition of the profiles of potential in the electrolyte solution, Φ_L and of the solid surface, Φ_S. Conditions for calculations given in text.

Experiments were carried out with the continuous recirculation of seawater or NaCl solution. The temperature in the two liquid circuits was controlled at 10 °C within 0.5 °C by means of heat exchangers (Figure 5). Two tanks were installed in the cathodic circuit to allow the electrolyte solution to be saturated with air oxygen supplied by gas spargers, and to be recycled after its treatment in the cell. The feeding tank with a volume of 18 litres, was installed 1.5 m above the electrolytic cell: the solution was continuously filtered and cooled before being fed into the cathode chamber. The liquid treated was driven to the 60 litre storage tank, before being pumped upward to the feeding tank.

The concentration of dissolved oxygen was continuously measured at the inlet and the outlet of the cell using amperometric probes with a response time below 60 s (WTW type, Microprocessor Oximeter OXI 325). The probes were immersed in 6 cm^3 glass stirred vessels for reliable values of the oxygen concentration.

3.3. *Experimental procedure and assessment of the selectivity*

The continuous oxygen removal from the solution was carried out in the potentiostatic mode and the current was continuously recorded. The cell voltage and the oxygen concentrations were also monitored by means of a data acquisition system provided with both digital and analog cards, and piloted by TestPoint™ software. All data were recorded every 15 s for a period of 15 min: the average values of the considered variables were calculated over this lapse of time and stored by the computer.

Because of the complex structure of the packed-bed electrode, with both external and internal porosities, the current was referred to the membrane area. The density at the membrane, i_M, defined as (I/A_M) was therefore used. The selectivity of the operation was assessed by defining the ratio η_F equivalent to a faradaic yield, considering the four-electron reduction of oxygen:

$$\eta_F = \frac{4F\dot{V}(C_{in} - C_{out})}{I} \tag{14}$$

A value for η_F close to unity expresses a four-electron process, and oxygen is reduced into water and hydroxide species. In case that the yield is near 2, peroxide production prevails at the electrode. Finally, a faradaic

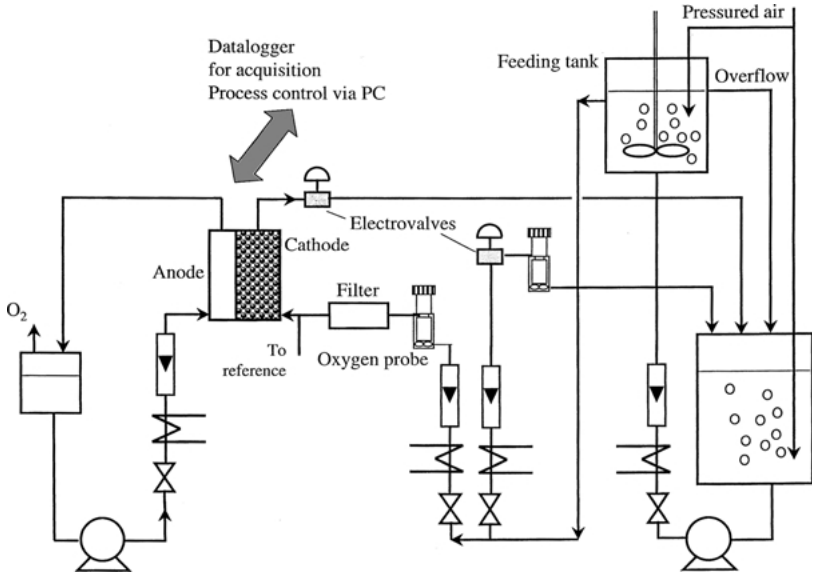

Fig. 5. Experimental set-up with the laboratory scale cell provide with the packed-bed electrode for the continuous reduction of dissolved oxygen.

yield below unity corresponds to significant hydrogen production.

4. Short-term experiments with NaCl solutions

These experiments were carried out with solutions of pure NaCl at 32.1 g l^{-1} at 10 °C. They were aimed at determining the selectivity of the reduction depending on the nature of the carbon-based material, and in relation to the current–potential relationship.

4.1. *Steady-state voltammetric curves at the packed-bed cathode*

As shown in Figure 6(a), polarization of the packed-bed electrode is slow, with a regular increase of the current density i_M over a large range of potential. The electrode kinetics could not be determined from these curves because of the significant ohmic drop in the electrode potential. The comparison of the various curves shows that higher currents are recorded on the surface of activated carbons than on graphite packed-bed electrodes: this may be attributed to the much larger area offered by AC materials, even though only a small fraction of the BET area is actually accessible to faradaic processes.

In the case of pure carbon electrodes, appreciable reduction currents are observed from −0.6 to −1.1 V vs SCE, and the rise in current observed at higher polarization may be due to the onset of hydrogen evolution. The voltammetric curves recorded at Pt impregnated materials exhibit comparable profiles, but at less cathodic voltages. As a matter of fact, shifting the (i/E) curve of Pt-graphite by −350 mV results in a voltammetric curve quite close to that recorded on pure graphite (Figure 6(b)). The plateau observed near

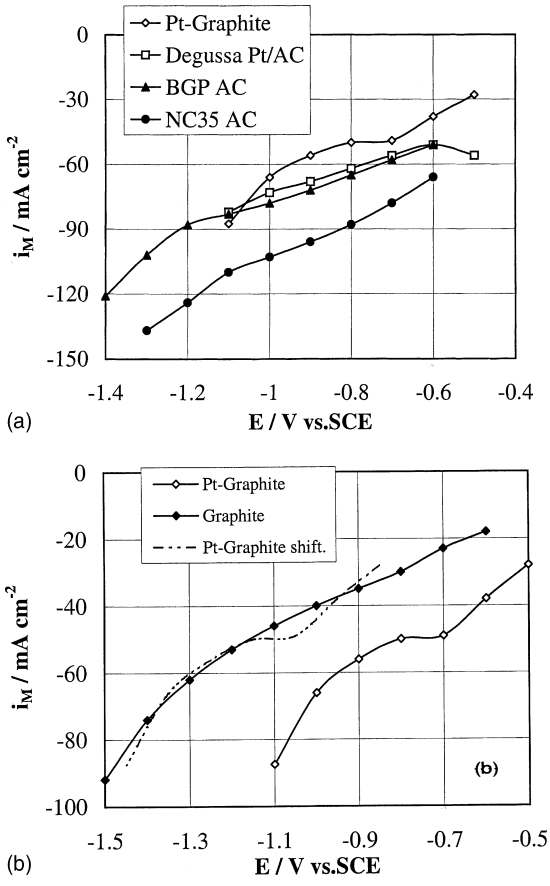

Fig. 6. Steady-state i_M/E curves recorded at the packed-bed electrode, depending on the catalyst employed. Superficial velocity 0.011 m s^{-1}. (a) Four different carbon-based materials were tested; (b) behaviour of graphite materials, depending on the presence of Pt at 1%. The dotted line refers to the i_M/E curve of Pt-graphite shifted by 350 mV.

−0.7 V vs SCE on the Pt/C surface may correspond to the diffusion-controlled reduction of oxygen into hydroxyl ions.

4.2. *Selectivity in the reduction of oxygen*

Transient decay of the current corresponding to capacitive phenomena at the electrode surface, was observed for periods ranging from twenty minutes to a few hours. Charging of the surface was particularly significant for materials exhibiting large BET areas such as AC.

The faradaic yield, η_F, of the reduction carried out on graphite was found to be about 1.8 in a large potential range (Figure 7). Above -1.0 V vs SCE a noticeable decrease of η_F was observed, indicating a more efficient reduction of the peroxide formed. This hypothesis of significant peroxide formation was confirmed by the use of a 400 cm^3 catalytic bed of Pt supported graphite installed between the cell and the outlet oxygen probe, in a bypass loop. At a given time, the liquid leaving the cell was allowed to percolate through the catalytic bed. After a delay corresponding to the mean residence time in the bed, the oxygen concentration in the treated solution was increased by approx. 0.5 mg l^{-1}, corresponding to the disproportionation of the peroxide produced in the electrochemical cell.

Values for η_F close to unity were obtained in the presence of Pt on the graphite surface (Figure 7) corresponding to the complete reduction of oxygen. The behaviour of activated carbon is somewhat intermediate, with η_F ranging from 1.1 to 1.25: both two and four-electron reductions occur in the cell. Again, the presence of Pt, as for the Degussa catalyst allows appreciable reduction of the yield. For all of the materials investigated, far cathodic polarisation of the packed bed electrode resulted in the formation of hydrogen, as indicated by η_F values below unity.

4.3. *Evidence of diffusion-controlled operation*

At sufficient polarization of the packed-bed, the current increases with the flow rate of the NaCl solution. The influence of the liquid velocity on the current was investigated at fixed potential corresponding to diffusion-controlled operation: E was fixed at -0.8 V with the Pt-graphite material and at -1.1 V with AC NC 35. The current could be fitted to the superficial velocity in the range investigated (Figure 8): I varied with $v^{0.37}$ for the Pt-graphite, and with $v^{0.40}$ for the activated carbon. Again, higher currents are recorded at the activated carbon due to its higher electrode area. In spite of the reduced range of velocity, the variations observed are fairly consistent with mass transfer correlations. The limiting current was calculated as a function of v and considering the external area of the packed bed, using Relations 7, 9 and 13. For this purpose, I_L was calculated on the basis of the inlet concentration of oxygen, the particles were considered as 2.5 mm beads, and four electrons were involved in the electrochemical reduction. The fair agreement between theory and practice showed that the reduction of O_2 is controlled by the rate of diffusion–convection at the particles, and that the active area of the bed is comparable to the external area of the bed.

5. Long-term experiments

5.1. *Tests with the Pt–AC catalyst*

Continuous runs were carried out for 160 h, first using the Degussa catalyst at -0.8 V vs SCE, allowing the reduction to be diffusion-controlled. The flow velocity was fixed at 0.011 m s^{-1}. After a rapid decay during the first hours, a regular decrease of the current was observed (Figure 9): the current density passed from 57 A m^{-2} after 10 h to 27 A m^{-2} at the end of the run. The cell voltage varied from 2.6 to 3.0 V. Yield η_F slowly increased to 1.3 after about 80 h and remained constant thereafter (Figure 9), which is in contradiction to the values near unity observed with the NaCl solution (Section 4).

The observed decrease of efficiency of the catalyst material could be attributed either to the loss of Pt from

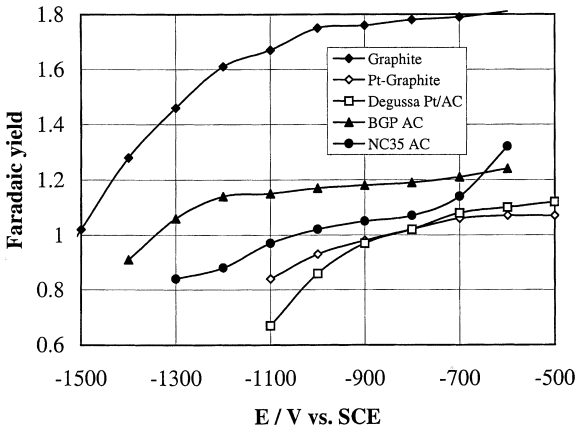

Fig. 7. Faradaic yield of the oxygen reduction versus the applied potential, depending on the nature of the carbon-based catalyst.

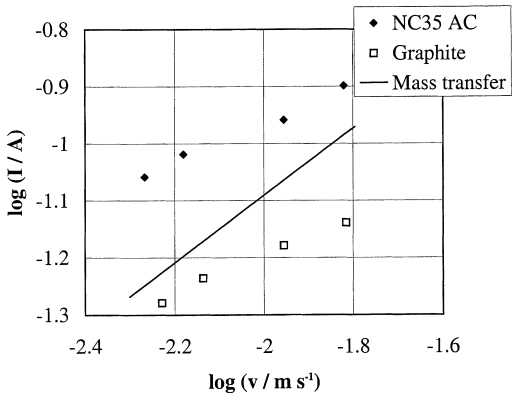

Fig. 8. Logarithmic plot of the current versus the superficial velocity of the liquid. The current corresponding to mass transfer control was calculated on the basis of the external surface of 2.5 mm spheres in the bed with an external porosity at 40%. The current recorded on the bed surface is compared with the theoretical one assuming mass transfer control.

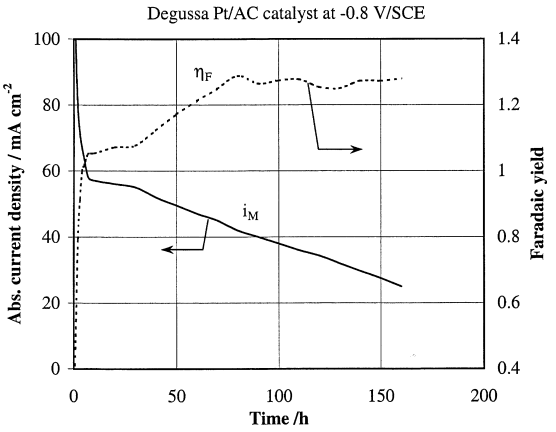

Fig. 9. Time variations of membrane current density, i_M, and of faradaic yield in the cell operated for 160 h; Pt–AC (Degussa) material; Applied potential −0.8 V vs SCE.

the catalyst material, or to the growth of a white deposit on the particles, as observed at the end of the run. Experiments were repeated for periods ranging from 10 to 60 h. After incineration of the carbonaceous support, the solid residue was extracted by aqua regia. The nitrous species were eliminated prior to analysis. The Pt content was determined by a spectrophotometric technique [16]; other cations were analysed by atomic absorption spectroscopy using a Varian AA20 instrument.

The loss of platinum from the catalyst was shown to be negligible. In contrast, analysis by AAS showed the regular increase in calcium and magnesium contents of the catalyst residues, attaining respectively 0.34 and 0.64 wt % after 160 h. Deposition of transition metal species on the catalyst was also put into evidence, with weight contents at 300 ppm for Fe, and around 20 ppm for Ni and Cu.

5.2. *Nature of the inhibiting film*

The electrochemical reduction of one mole of oxygen involves the formation of four moles of hydroxyl ions resulting in an increase of the pH at the electrode surface. In a first approach we may neglect the possible formation of metal hydroxides, due to the buffering character of seawater, and the mass balance at distance y from the inlet of the cell may be written as

$$\sum_i v_i \frac{\mathrm{d}n_i(y)}{\mathrm{d}t} = 0 \quad \text{with } i = \mathrm{O_2}, \mathrm{H_2O} \text{ and } \mathrm{OH^-} \qquad (15)$$

where the stoichiometric coefficients v_i refer to the reduction of oxygen into OH^-. Assuming that the reduction is diffusion-rate controlled, the Nernst film model leads to

$$\frac{\mathrm{d}n_i(y)}{\mathrm{d}t} = \frac{D_i}{\delta} a (C_i(y) - C_i^*(y)) \qquad (16)$$

where δ is the thickness of the film and C^* refers to the surface concentration. The change in water concentration can be neglected, and Relations 15 and 16 yield:

$$C^*_{\mathrm{OH^-}} = C_{\mathrm{OH^-}} + \frac{4D_{\mathrm{O_2}}}{D_{\mathrm{OH^-}}} C_{\mathrm{O_2}} \qquad (17)$$

where we consider that the concentration of dissolved oxygen at the surface is reduced to zero. The diffusivity of OH^- under the operating conditions can be deduced from its value in pure water at 25 °C, taking into account the change in temperature and viscosity, and can be estimated to 3.1×10^{-9} m^2 s^{-1}. The value of $C^*_{\mathrm{OH^-}}$ merely depends on the concentration of oxygen and for an average value of 8 ppm in the packed bed, application of Relation 17 leads to an interfacial pH of about 10.7. We may now estimate the possible formation of solids at the catalyst surface by calculation of the protolytic equilibria in the system water–carbonate–Ca(II)–Mg(II). This had been done by use of the data listed in Table 4 [17, 18], neglecting the deviation from 25 °C [19].

From the concentrations of magnesium and calcium cations given in Table 2, solid magnesium hydroxide is formed for pH above 9.3, and calcium carbonate appears from pH around 8. In spite of the assumptions made in the approach, the solid formed at the surface of the packed bed particles was shown to be calcium carbonate and magnesium hydroxide. These solid salts block the active sites of the catalyst, hindering the decomposition of hydrogen peroxide species and results in higher η_F values. In addition, insoluble hydroxides of iron, nickel and copper could also be formed, although to far lower amounts.

Experiments with NaCl solutions at the same ionic strength and saturated with oxygen, showed no current decay for 90 h, with η_F values in the range 1.0–1.05, which confirms the above interpretation of the inhibition.

5.3. *Further long-term runs*

Experiments were conducted with the Degussa Pt–AC catalyst for 160 h at −1.0 V vs SCE. The membrane current density remained in the range 55–75 A m^{-2} with day-period fluctuations (Figure 10). The faradaic yield

Table 4. Equilibria involved in the Ca(II)–Mg(II)–carbonate–water system and related pK values at 25 °C [17, 18]

Equilibrium	pK
$H_2O \longleftrightarrow H^+ + OH^-$	14
$H_2O + CO_2 \longleftrightarrow HCO_3^- + H^+$	6.4
$HCO_3^- \longleftrightarrow CO_3^{2-} + H^+$	10.3
$Ca^{2+} + H_2O \longleftrightarrow Ca(OH)^+ + H^+$	12.7
$CaCO_{3\ sol} \longleftrightarrow Ca^{2+} + CO_3^{2-}$	7.6
$Ca(OH)_{2\ sol} \longleftrightarrow Ca^{2+} + 2\ OH^-$	5.26
$Mg^{2+} + H_2O \longleftrightarrow Mg(OH^+) + H^+$	11.4
$Mg(OH)_{2\ sol} \longleftrightarrow Mg^{2+} + 2\ OH^-$	10.74

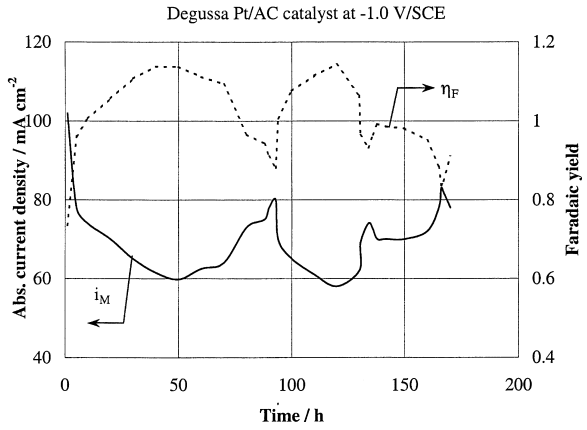

Fig. 10. Time variations of membrane current density, i_M, and of faradaic yield in the cell operated for 170 h; Pt–AC (Degussa) material; Applied potential −1.0 V vs SCE.

η_F varied from 0.95 to 1.15, with an average value at 1.06. A slight gas evolution was observed throughout the run: its analysis by mass spectrometry and flame testing showed the predominant presence of nitrogen and oxygen, with negligible hydrogen content. The gas evolution may be due to degassing of the catalyst particles and/or of the seawater. The aspect of the packed-bed remained unchanged but a white deposit was observed close to the membrane: the chemical analysis of the solid revealed the presence of magnesium and calcium in a 2.8 ratio, comparable with the 3.3 ratio in seawater. The gas evolution, in spite of its moderate significance, seems to prevent the deposition of solid calcium and magnesium salts on the carbon particles, resulting in the negligible coverage of their surface.

BGP activated carbon, without platinum, was also tested for 240 h and the potential was fixed at −1.1 V vs SCE. The membrane current density was 75 A m^{-2} within 10% during the tenday test (Figure 11), as for the shorter runs presented in Section 4. The faradaic yield remained in the range 1.15–1.25, corresponding to the values presented in Figure 7.

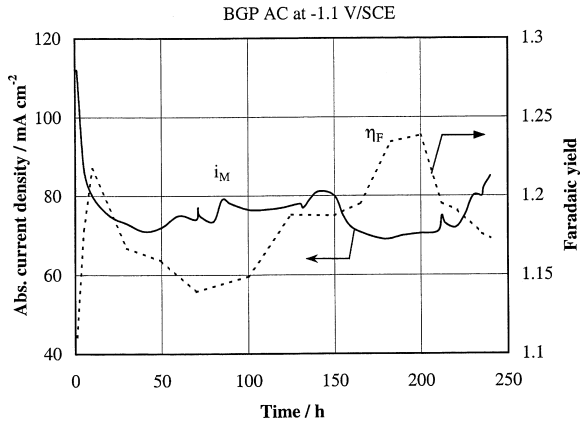

Fig. 11. Time variations of membrane current density, i_M, and of faradaic yield in the cell operated for 235 h; BGP Activated carbon; Applied potential −1.1 V vs SCE.

6. Conclusion and significance

The electrochemical reduction of oxygen from seawater can be carried out with appreciable yields at a packed-bed electrode of carbon-based particles. In contrast to pure carbon materials, platinum-impregnated carbons allow the fast complete reduction of oxygen into hydroxyl ions. The presence of magnesium and calcium salts in seawater was shown to be the possible source of deactivation of the catalysts by the formation of a solid film of calcium carbonate and magnesium hydroxide, due to the local increase of pH. The phenomenon can be of moderate significance with further polarization of the cathode. In addition, it is hoped that the deactivation of the catalyst particle caused by the local increase in pH, should not occur for sufficient reduction extent of the dissolved oxygen, as required for the treatment of seawater for off-shore exploitations.

The results presented here were used for the design and the construction of a pilot plant allowing 80% abatement of dissolved oxygen from seawater pumped at 180 l h^{-1}. The tests conducted over a two-month period showed the feasibility of the technique with constant current and oxygen conversion within 10% [19]. Now, the design of the electrocatalytic reactor for the treatment of 5000 m^3 of seawater per day, and the economical and technological analysis of the overall process are under investigation.

Acknowledgement

Thanks are due to Total Fina-Elf, France, who sponsored the investigation and covered the PhD grant to P. Kinzel.

References

1. L.A. Cantu, M.E. Yost, R.L. Coffee and J.E. Stohland, *US Patent* 4 527 626 (1985).
2. 'Water Treatment Handbook', Degrémont, Lavoisier, Paris (1991).
3. C. Zheng, K. Guo, Y. Song, X. Zhou, D. Hai, Z. Xin and N.C. Gardner, Proc. 2nd Int. Conf. Proc. Intensif. in Practice, 28, BHR Group, London, (1997), pp. 273–87.
4. J. Barbier and K. Nohair, Internal report, Lab. Catal. Chimie Organique, CNRS–Université Poitiers (1996).
5. A.S. Elf-Norge, Internal report (1997).
6. A. Vieira Nunes, PhD dissertation, INPL, Nancy (1999).
7. K. Kinoshita, 'Carbon, Electrochemical and Physicochemical Properties' (J. Wiley & Sons, New York, 1988).
8. M.R. Tarasevich and E.I. Khrusheva, *in* B.E. Conway, J.O'M. Bockris and R.E. White (Eds), 'Modern Aspects of Electrochemistry', Vol. 19 (Plenum Press, New York, 1989), pp. 285–358.
9. L. Ginest-Bultel, PhD dissertation, INPG, Grenoble (1997).
10. M.R. Tarasevich, A. Sadkowski and E. Yeager, 'Oxygen electrochemistry', *in* 'Comprehensive Treatise of Electrochemistry, Kinetics and Mechanisms of Electrode Processes' (Plenum, New York, 1983), p. 301.
11. J. Perez, A.A. Tanaka, E.R. Gonzalez and E.A. Ticianelli, *J. Electrochem. Soc.* **141** (1994) 431.
12. M.A. Enriquez-Granados, PhD dissertation, INPL, Nang (1982). See also A. Storck et al. *Electrochim. Acta* **23** (1983) 1407.

13. G. Valentin, M. Giron, A. Storck and J.P. Guerlet, 'Un nouveau réacteur électrochimique' pour la récupération d'argent dans les bains de fixage photographique', *Rev. Gen. Electricité* (in French), no. 3 (1992).
14. P.N. Dwidedi and S.N. Upadhay, *I.E.C. Process Design Dev*. **16**(2) (1977) 157.
15. M.S. Hossain, D. Tryk and E. Yeager, *Electrochim. Acta* **34** (1989) 1733.
16. H-G. Lintz, *Ind. Eng. Chem. Res*. **30** (1991) 2012 (also see I. Maziekien, L. Ermanis and T.J. Walsh, *Anal. Chem*. **32** (1960) 645).
17. A. Ringbom, 'Complexation in Analytical Chemistry' (Interscience Publishers, London, 1963).
18. S. Kotrly and L. Sucha, 'Handbook of Chemical Equilibria in Analytical Chemistry' (Ellis Horwood, Chichester, UK 1985).
19. P. Kinzel, PhD dissertation, INPL, Nancy (1999).